# Towards UAV-USV Collaboration in Harsh Maritime Conditions Including Large Waves

Filip Novák[a], Tomáš Báča[b], Ondřej Procházka[c] and Martin Saska[d]
*Department of Cybernetics, Faculty of Electrical Engineering, Czech Technical University in Prague, Czech Republic*
*fi*

Keywords: Unmanned Aerial Vehicle, Unmanned Surface Vehicle, Boat Dynamics, Boat Model, State Estimation.

Abstract: This paper introduces a system designed for tight collaboration between Unmanned Aerial Vehicles (UAVs) and Unmanned Surface Vehicles (USVs) in harsh maritime conditions characterized by large waves. This onboard UAV system aims to enhance collaboration with USVs for following and landing tasks under such challenging conditions. The main contribution of our system is the novel mathematical USV model, describing the movement of the USV in 6 degrees of freedom on a wavy water surface, which is used to estimate and predict USV states. The estimator fuses data from multiple global and onboard sensors, ensuring accurate USV state estimation. The predictor computes future USV states using the novel mathematical USV model and the last estimated states. The estimated and predicted USV states are forwarded into a trajectory planner that generates a UAV trajectory for following the USV or landing on its deck, even in harsh environmental conditions. The proposed approach was verified in numerous simulations and deployed to the real world, where the UAV was able to follow the USV and land on its deck repeatedly.

## 1 INTRODUCTION

The Unmanned Aerial Vehicles (UAVs) have already proven their efficiency in numerous marine applications. The UAVs are helpful in search and rescue operations (Murphy et al., 2008), monitoring marine animals (Aniceto et al., 2018), monitoring water quality (Román et al., 2023), or cleaning oceans from garbage and oil spills (Han and Ma, 2021). However, the UAVs are limited by short battery life, which reduces their operational time. This limitation is problematic as marine tasks are often executed at long distances from offshore base stations. Therefore, the UAVs often collaborate with the Unmanned Surface Vehicles (USVs) (Han and Ma, 2021; Murphy et al., 2006), which can compensate for UAVs short battery life by power umbilical tether (Talke et al., 2018) or providing docking spot for battery recharging (Aissi et al., 2020).

In order to provide power supply via an umbilical tether from the USV to the UAV, the UAV has to precisely follow the USV at the specified distance based on the tether length (Talke et al., 2018), which requires estimating and predicting USV movement even in harsh conditions such as rough waters with large waves. Similarly, estimating and predicting USV movement is crucial for the UAV during landing on the USV docking spot (Gupta et al., 2023). The oscillating and tilting USV on a wavy water surface can significantly damage the landing UAV or even cause UAV to fall into the water.

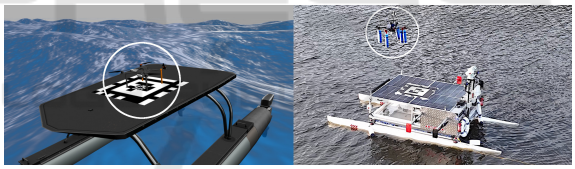

Figure 1: The tight collaboration between UAVs (marked with white circles) and USVs during the landing and following tasks using our system presented in this paper.

The approach proposed in this paper allows tight collaboration between UAVs and USVs (see Fig. 1), such as following and landing tasks on rough water surfaces. The key component of the presented system is the USV state estimator, which runs onboard the UAV and fuses data from the onboard sensors of both robots. Using a novel mathematical USV model containing wave dynamics, the estimated states are used to predict future USV movement on the wavy water

[a] https://orcid.org/0000-0003-3826-5904
[b] https://orcid.org/0000-0001-9649-8277
[c] https://orcid.org/0009-0009-2224-750X
[d] https://orcid.org/0000-0001-7106-3816



Novák, F., Báča, T., Procházka, O. and Saska, M.
Towards UAV-USV Collaboration in Harsh Maritime Conditions Including Large Waves.
DOI: 10.5220/0012910000003822
In *Proceedings of the 21st International Conference on Informatics in Control, Automation and Robotics (ICINCO 2024) - Volume 1*, pages 545-554
ISBN: 978-989-758-717-7; ISSN: 2184-2809

surface. The estimated and predicted USV states enable precise UAV trajectory planning for following and landing. The proposed approach was verified in numerous simulations and real-world experiments in both use cases: following the USV and landing on the USV docking spot.

The main paper contributions are summarized in the following points:

- We propose a novel linear USV mathematical model containing wave dynamics that enables accurate estimation and prediction of the USV movement on wavy water surface in 6 Degrees of Freedom (DOFs).
- We introduce a novel onboard UAV system to tight collaboration between UAVs and USVs in following and landing tasks in harsh maritime conditions, including large waves.

## 2 RELATED WORKS

The works (Meng et al., 2019; Lee et al., 2019) propose solutions for the following and landing of fixed-wing UAVs on marine vessels. The method presented in (Meng et al., 2019) uses the auto-regressive model to predict the landing pad position at the touchdown moment. The landing pad is equipped with infrared targets that are detected onboard UAV to measure the relative position of the landing pad. The approach (Lee et al., 2019) relies on a sliding-mode control scheme to guide the UAV towards the landing point by following a desired reference trajectory. The position of the landing point at touchdown time is predicted to be used in the final phase of the landing. However, neither of these methods has been verified through real-world experiments, and the harsh environment is not considered in simulations.

An internal-model-based approach for Vertical Take-Off and Landing (VTOL) UAVs is introduced in (Marconi et al., 2002). This approach is designed for autonomous landing on a vertically oscillating deck. The oscillations of the deck are modeled as a sum of sinusoidal functions. However, the oscillations are considered only in heave motion. The approach does not consider the pitch and roll motions of the landing deck. Furthermore, the approach is not deployed in the real world, and its validation is limited to simulations.

A visual-based autonomous landing of UAV on a moving USV is presented in (Keller and Ben-Moshe, 2022). The method (Keller and Ben-Moshe, 2022) relies only on the position of the landing platform. However, it's important to note that this method does not account for the roll and pitch motions during landing, which can pose a risk, particularly in rough water conditions where the rolling and pitching of the landing platform may potentially damage the UAV. Although the method (Keller and Ben-Moshe, 2022) is verified in real-world experiments, the method is not designed for harsh environments. A similar vision-based approach is presented in (Venugopalan et al., 2012). This approach also considers only USV position as (Keller and Ben-Moshe, 2022) and is deployed in the real world. Neither methods (Keller and Ben-Moshe, 2022; Venugopalan et al., 2012) analyze waves influencing the USV motions, which does not make them prepared for harsh conditions.

The method for following and landing verified in the real world is presented in (Xu et al., 2020). In this method, the UAV uses a camera to detect a tag placed on the landing platform, which is placed onboard USV. The detected tag is then used to estimate the relative position from the UAV to the USV. A similar estimation method is also employed in (Yang et al., 2021). Both methods are verified by conducting real-world experiments. However, harsh conditions, such as large waves, as well as pitch and roll motions of the USV, are not considered in these methods.

The complex system estimating USV motion in 5 DOFs is proposed in (Abujoub et al., 2018). The estimation method differs from previous vision-based approaches by utilizing Light Detection and Ranging (LiDAR) to measure the position and orientation of the USV. Additionally, the future roll and pitch motions are predicted as the sum of harmonic functions representing the wave motions. The parameters of these harmonic functions are derived from Fast Fourier Transform (FFT) of estimated roll and pitch angles. However, this method does not consider wave motion in the heave state of the USV, which could potentially lead to unsafe landing or following, especially in rough conditions. Furthermore, the method is solely tested in simulations and has not been validated in real-world experiments.

The above-mentioned methods (Keller and Ben-Moshe, 2022; Venugopalan et al., 2012; Xu et al., 2020; Yang et al., 2021; Abujoub et al., 2018) rely solely on vision methods to estimate USV states. However, a significant limitation of these methods arises when the USV falls outside the Field of View (FOV) of the UAV sensors, rendering it impossible to estimate the position and orientation of the USV. In such cases, the UAV must actively search for the USV, leading to increased energy consumption and limiting the time dedicated to the UAV mission. An alternative approach, as presented in (Zhang et al., 2021), combines Global Navigation Satellite System

(GNSS) sensors placed on the USV with onboard UAV vision-based systems to estimate the position of the USV. However, it's important to note that neither the orientation of the USV nor wave motions are accounted for in the estimation process. Consequently, the method presented in (Zhang et al., 2021) is deemed unsuitable for harsh conditions.

The method proposing USV state estimation in full 6 DOFs is presented in (Polvara et al., 2018). The UAV detects the tag placed on USV board in camera images and utilizes it for the estimation. Subsequently, the method controls the UAV landing on the USV board. However, the waves are not considered for any USV state, making the method unsuitable for harsh conditions that are considered in this paper. The method for landing UAV on USV in harsh conditions is presented in (Gupta et al., 2023). The method considers waves in the USV motion and predicts future USV states to perform a safe landing. However, the assumption made in (Gupta et al., 2023) that the USV is not moving horizontally on the water surface renders the method unsuitable for the task of UAV following. Additionally, both methods (Polvara et al., 2018; Gupta et al., 2023) are purely vision-based, causing aforementioned issues if the USV is not in the FOV of the UAV onboard sensors.

In comparison with the above-mentioned methods, our system integrates both USV onboard sensors and UAV onboard sensors to accurately estimate the USV motion in full 6 DOFs, while factoring in wave dynamics at every state. Additionally, our system predicts the future USV states in 6 DOFs, incorporating wave motions. Therefore, our system enables tight UAV-USV collaboration in extreme environmental conditions at different relative UAV-USV distances constrained by the communication range. The estimated and predicted USV states serve as inputs to the UAV trajectory planner, based on the Model Predictive Control (MPC) method, enabling the UAV to follow the USV and land on it even in harsh environmental conditions.

## 3 MATHEMATICAL USV MODEL

We identify accurate state estimation and prediction of USV states as crucial features for tight UAV-USV collaboration, enabling the UAV to follow the USV and land on its deck even in harsh conditions, including large waves. In this section, we present a novel linear USV model containing wave dynamics in order to fuse data from multiple sensors, thereby increasing estimation and prediction accuracy. We model the USV in 6 DOFs, consisting of 3D translation (surge $x$, sway $y$, and heave $z$) and 3D rotation in terms of intrinsic Euler angles (roll $\phi$, pitch $\theta$, and yaw $\psi$), as illustrated in Fig. 2.

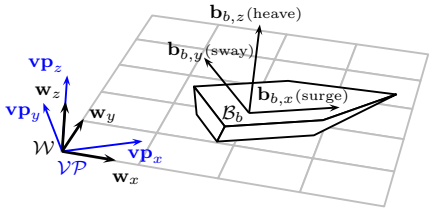


Figure 2: The depiction of the world frame $\mathcal{W} = \{\mathbf{w}_x, \mathbf{w}_y, \mathbf{w}_z\}$, Vessel parallel coordinate system $\mathcal{VP} = \{\mathbf{vp}_x, \mathbf{vp}_y, \mathbf{vp}_z\}$, and USV body-fixed coordinate frame $\mathcal{B}_b = \{\mathbf{b}_{b,x}, \mathbf{b}_{b,y}, \mathbf{b}_{b,z}\}$.

In order to analyze the USV motion, three coordinate frames are presented: the world coordinate frame $\mathcal{W} = \{\mathbf{w}_x, \mathbf{w}_y, \mathbf{w}_z\}$, the body-fixed coordinate frame $\mathcal{B}_b = \{\mathbf{b}_{b,x}, \mathbf{b}_{b,y}, \mathbf{b}_{b,z}\}$, and the Vessel parallel coordinate frame $\mathcal{VP} = \{\mathbf{vp}_x, \mathbf{vp}_y, \mathbf{vp}_z\}$ as shown in Fig. 2. The position $\boldsymbol{p}_L = (x_L, y_L, z_L)^\intercal$ and rotation $\boldsymbol{\Theta}_L = (\phi_L, \theta_L, \psi_L)^\intercal$ of the USV are expressed in the Vessel parallel coordinate frame $\mathcal{VP}$, which is parallel to the body-fixed coordinate frame $\mathcal{B}_b$ and placed at the origin of the world coordinate frame $\mathcal{W}$. The USV state, expressed in Vessel parallel coordinate frame $\boldsymbol{\eta}_L = (\boldsymbol{p}_L^\intercal, \boldsymbol{\Theta}_L^\intercal)^\intercal$, is transformed to the world coordinate frame as $\boldsymbol{\eta} = (\boldsymbol{p}^\intercal, \boldsymbol{\Theta}^\intercal)^\intercal$ as

$$\boldsymbol{\eta} = \mathbf{J}_\psi(\psi)\boldsymbol{\eta}_L, \tag{1}$$

where transformation matrix $\mathbf{J}_\psi(\psi)$ is defined as

$$\mathbf{J}_\psi(\psi) = \begin{pmatrix} \mathbf{R}_\psi & \mathbf{O}_{3\times3} \\ \mathbf{O}_{3\times3} & \mathbf{I}_{3\times3} \end{pmatrix}, \tag{2}$$

$$\mathbf{R}_\psi = \begin{pmatrix} \cos\psi & -\sin\psi & 0 \\ \sin\psi & \cos\psi & 0 \\ 0 & 0 & 1 \end{pmatrix}, \tag{3}$$

$\mathbf{O}_{3\times3} \in \mathbb{R}^{3\times3}$ is a zero matrix, and $\mathbf{I}_{3\times3} \in \mathbb{R}^{3\times3}$ denotes the identity matrix. The Vessel parallel coordinate frame $\mathcal{VP}$ enables us to use an identity matrix as the transformation between velocity state vector $\boldsymbol{\nu}$ and the derivative of vector $\boldsymbol{\eta}_L$. The linear velocity $\boldsymbol{v} = (u, v, w)^\intercal$ and angular velocity $\boldsymbol{\omega} = (p, q, r)^\intercal$ form the state vector $\boldsymbol{\nu} = (\boldsymbol{v}^\intercal, \boldsymbol{\omega}^\intercal)^\intercal$, expressed in the body-fixed coordinate frame $\mathcal{B}_b$.

Our novel USV model builds upon the USV motion analysis presented in (Fossen, 2011) and extends it by wave dynamics, resulting in a mathematical model that describes the USV motion on a rough water surface. First, the equations of USV motions are

$$\dot{\boldsymbol{\eta}}_L = \boldsymbol{\nu}, \tag{4}$$

$$\dot{\boldsymbol{\nu}} = (\mathbf{M}_I + \mathbf{M}_A)^{-1}(-\mathbf{D}\boldsymbol{\nu} - \mathbf{G}\boldsymbol{\eta}_L), \tag{5}$$

where $\mathbf{M}_I \in \mathbb{R}^{6\times6}$ represents the inertia matrix, the $\mathbf{M}_A \in \mathbb{R}^{6\times6}$ is hydrodynamic added mass occurring due to the motion of the USV through the fluid. The matrix $\mathbf{D} \in \mathbb{R}^{6\times6}$ represents the linear damping and term $\mathbf{G} \in \mathbb{R}^{6\times6}$ denotes matrix of gravitational forces and torques, also called restoring forces.

We assume the waves as an oscillatory motion in each USV state. Therefore, we present one wave component as a 2 DOF linear state-space model, defined by matrices $\mathbf{A}_\omega$, $\mathbf{C}_\omega$ as

$$\begin{pmatrix} \dot{x}_{\omega_1} \\ \dot{x}_{\omega_2} \end{pmatrix} = \underbrace{\begin{pmatrix} 0 & 1 \\ -\omega_0^2 & -2\lambda\omega_0 \end{pmatrix}}_{\mathbf{A}_\omega} \begin{pmatrix} x_{\omega_1} \\ x_{\omega_2} \end{pmatrix}, \tag{6}$$

$$y_\omega = \underbrace{\begin{pmatrix} 0 & 1 \end{pmatrix}}_{\mathbf{C}_\omega} \begin{pmatrix} x_{\omega_1} \\ x_{\omega_2} \end{pmatrix}, \tag{7}$$

where $\boldsymbol{x}_\omega = (x_{\omega_1}, x_{\omega_2})^\intercal$ is a state of the wave component, $\lambda$ is a damping term, and $\omega_0$ denotes the frequency of the wave component. To model wave motion with complex frequency spectra, we combined $N_c \in \mathbb{Z}^+$ wave components from equations (6) and (7). Each component is characterized by different parameters $\lambda$ and $\omega_0$

$$\dot{\boldsymbol{x}}_{\omega_1} = \mathbf{A}_{\omega_1}\boldsymbol{x}_{\omega_1}, \tag{8}$$
$$y_{\omega_1} = \mathbf{C}_{\omega_1}\boldsymbol{x}_{\omega_1}, \tag{9}$$
$$\vdots$$
$$\dot{\boldsymbol{x}}_{\omega_{N_c}} = \mathbf{A}_{\omega_{N_c}}\boldsymbol{x}_{\omega_{N_c}}, \tag{10}$$
$$y_{\omega_{N_c}} = \mathbf{C}_{\omega_{N_c}}\boldsymbol{x}_{\omega_{N_c}}, \tag{11}$$
$$y_{\text{wave}} = y_{\omega_1} + \ldots + y_{\omega_{N_c}}. \tag{12}$$

The equations (8)-(12) can be expressed as

$$\dot{\boldsymbol{x}}_{\text{wave}} = \mathbf{A}_{\text{wave}}\boldsymbol{x}_{\text{wave}}, \tag{13}$$
$$y_{\text{wave}} = \mathbf{C}_{\text{wave}}\boldsymbol{x}_{\text{wave}}, \tag{14}$$
$$\boldsymbol{x}_{\text{wave}} = (\boldsymbol{x}_{\omega_1}^\intercal, \ldots, \boldsymbol{x}_{\omega_{N_c}}^\intercal)^\intercal, \tag{15}$$
$$\mathbf{A}_{\text{wave}} = \text{diag}\{\mathbf{A}_{\omega_1}, \ldots, \mathbf{A}_{\omega_{N_c-1}}\}, \tag{16}$$
$$\mathbf{C}_{\text{wave}} = \begin{pmatrix} \mathbf{C}_{\omega_1} & \cdots & \mathbf{C}_{\omega_{N_c}} \end{pmatrix}, \tag{17}$$

where $\text{diag}\{\cdot\}$ is a symbol for a block diagonal matrix created from the elements in the bracket. The wave model (13)–(14) is integrated into each state of the USV state vector $\boldsymbol{\nu}$. Hence, we present the complex model of waves influencing USV motion as

$$\dot{\boldsymbol{x}}_{\text{wave},\boldsymbol{\nu}} = \mathbf{A}_{\text{wave},\boldsymbol{\nu}}\boldsymbol{x}_{\text{wave},\boldsymbol{\nu}}, \tag{18}$$
$$\boldsymbol{y}_{\text{wave},\boldsymbol{\nu}} = \mathbf{C}_{\text{wave},\boldsymbol{\nu}}\boldsymbol{x}_{\text{wave},\boldsymbol{\nu}}, \tag{19}$$

where $\mathbf{A}_{\text{wave},\boldsymbol{\nu}}$ and $\mathbf{C}_{\text{wave},\boldsymbol{\nu}}$ are block diagonal matrices

$$\mathbf{A}_{\text{wave},\boldsymbol{\nu}} = \text{diag}\{\mathbf{A}_{\text{wave}}, \mathbf{A}_{\text{wave}}, \mathbf{A}_{\text{wave}}, \mathbf{A}_{\text{wave}}, \mathbf{A}_{\text{wave}}, \mathbf{A}_{\text{wave}}\}, \tag{20}$$

$$\mathbf{C}_{\text{wave},\boldsymbol{\nu}} = \begin{pmatrix} \mathbf{C}_{\text{wave}} & \mathbf{O}_{1\times2N_c} & \cdots & \mathbf{O}_{1\times2N_c} \\ \mathbf{O}_{1\times2N_c} & \ddots & \ddots & \vdots \\ \vdots & \ddots & \mathbf{C}_{\text{wave}} & \mathbf{O}_{1\times2N_c} \\ \mathbf{O}_{1\times2N_c} & \cdots & \mathbf{O}_{1\times2N_c} & \mathbf{C}_{\text{wave}} \end{pmatrix}, \tag{21}$$

and

$$\boldsymbol{x}_{\text{wave},\boldsymbol{\nu}} = (\boldsymbol{x}_{\text{wave},u}^\intercal, \boldsymbol{x}_{\text{wave},v}^\intercal, \boldsymbol{x}_{\text{wave},w}^\intercal, \boldsymbol{x}_{\text{wave},p}^\intercal, \boldsymbol{x}_{\text{wave},q}^\intercal, \boldsymbol{x}_{\text{wave},r}^\intercal)^\intercal. \tag{22}$$

Finally, the novel 6 DOF mathematical model of the USV containing wave dynamics is

$$\dot{\boldsymbol{x}}_{\text{usv}} = \mathbf{A}_{\text{usv}}\boldsymbol{x}_{\text{usv}}, \tag{23}$$

where $\boldsymbol{x}_{\text{usv}} = (\boldsymbol{\eta}_L^\intercal, \boldsymbol{\nu}^\intercal, \boldsymbol{x}_{\text{wave},\boldsymbol{\nu}}^\intercal)^\intercal$,

$$\mathbf{A}_{\text{usv}} = \begin{pmatrix} \mathbf{O}_{6\times6} & \mathbf{I}_{6\times6} & \mathbf{O}_{6\times12N_c} \\ -\mathbf{M}^{-1}\mathbf{G} & -\mathbf{M}^{-1}\mathbf{D} & \mathbf{C}_{\text{wave},\boldsymbol{\nu}} \\ \mathbf{O}_{12N_c\times6} & \mathbf{O}_{12N_c\times6} & \mathbf{A}_{\text{wave},\boldsymbol{\nu}} \end{pmatrix}, \tag{24}$$

and $\mathbf{M} = \mathbf{M}_I + \mathbf{M}_A$.

# 4 UAV-USV COLLABORATION IN WAVES

The pipeline integrating the entire UAV-USV system is depicted in Fig. 3. The pipeline comprises three main areas – USV plant, UAV plant, and the proposed approach for tight UAV-USV collaboration. The USV plan consists of a Global Positioning System (GPS) sensor and an Inertial Measurement Unit (IMU), whose data are sent to our state estimator. The UAV plant includes onboard sensors – AprilTag detector (Olson, 2011; Wang and Olson, 2016; Krogius et al., 2019), and UltraViolet Direction And Ranging (UVDAR) system (Walter et al., 2020; Walter et al., 2018b; Walter et al., 2018a), which are discussed later in this paper. The UAV is controlled by the Multi-robot Systems (MRS) UAV system (Baca et al., 2021), enabling precise following of a trajectory planned by the proposed method. The State estimator that fuses data from USV and UAV onboard sensors using a novel mathematical USV model (23) to obtain an accurate estimate of USV states moving on rough water surfaces. The estimated states and novel mathematical model are then used in the State predictor to predict future USV states. The estimated and predicted USV states are forwarded to the Trajectory planner, which generates a UAV trajectory to follow the USV and land on its deck.

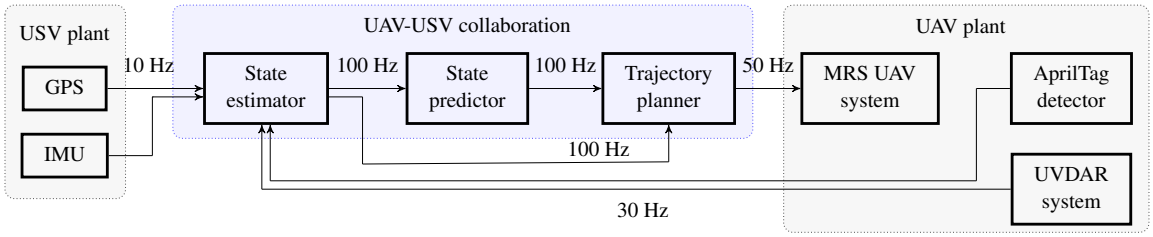


Figure 3: The figure depicts a pipeline diagram of the entire system used for experimental verification in this paper. The *State estimator* fuses data from USV onboard sensors (GPS and IMU) and UAV onboard sensors (AprilTag detector and UVDAR system). The estimated USV states are then sent to the *State predictor*, which predicts future USV states. The *Trajectory planner* uses the estimated and predicted USV states to generate a UAV trajectory, which is precisely tracked by the *MRS UAV system* (Baca et al., 2021).

## 4.1 State Estimator and Predictor

We rely on the Linear Kalman Filter (LKF) (Kalman, 1960) as the state estimator, utilizing a discrete version $\mathbf{A}_{\text{usv},d}$ of our novel linear USV model (23). The LKF consists of two main steps: the prediction step and the correction step. The prediction step uses the last estimated USV state and propagates it through the mathematical model to obtain a new state

$$\boldsymbol{x}_{\text{usv}}(k+1) = \mathbf{A}_{\text{usv},d}\boldsymbol{x}_{\text{usv}}(k), \tag{25}$$

$$\mathbf{P}_{\text{usv}}(k+1) = \mathbf{A}_{\text{usv},d}\mathbf{P}_{\text{usv}}(k)\mathbf{A}_{\text{usv},d}^{\mathsf{T}} + \mathbf{Q}_{\text{usv}}, \tag{26}$$

where $k \in \mathbb{Z}^+$ is a time step, $\mathbf{P}_{\text{usv}}(k) \in \mathbb{R}^{12(1+N_c)\times 12(1+N_c)}$ stands for covariance matrix of USV state $\boldsymbol{x}_{\text{usv}}(k)$, and $\mathbf{Q}_{\text{usv}} \in \mathbb{R}^{12(1+N_c)\times 12(1+N_c)}$ represents a system noise matrix. The correction step incorporates incoming measurement $\boldsymbol{z}(k)$ to update the last estimated state

$$\boldsymbol{x}_{\text{usv}}(k) = \boldsymbol{x}_{\text{usv}}(k) + \mathbf{G}(k)\left(\boldsymbol{z}(k) - \mathbf{C}\boldsymbol{x}_{\text{usv}}(k)\right), \tag{27}$$

$$\mathbf{P}_{\text{usv}}(k) = \mathbf{P}_{\text{usv}}(k) - \mathbf{G}(k)\mathbf{C}\mathbf{P}_{\text{usv}}(k), \tag{28}$$

$$\mathbf{G}(k) = \mathbf{P}_{\text{usv}}(k)\mathbf{C}^{\mathsf{T}}\left(\mathbf{C}\mathbf{P}_{\text{usv}}(k)\mathbf{C}^{\mathsf{T}} + \mathbf{R}\right)^{-1}, \tag{29}$$

where $\mathbf{R}$ is measurement noise matrix, and matrix $\mathbf{C}$ represents mapping between state $\boldsymbol{x}_{\text{usv}}$ and measurement $\boldsymbol{z}$. To predict future USV states from the last estimated values $\boldsymbol{x}_{\text{usv}}(k)$ and $\mathbf{P}_{\text{usv}}(k)$, the prediction step of the LKF is iteratively applied to obtain $N_p \in \mathbb{Z}^+$ number of predictions

$$\hat{\boldsymbol{x}}_{\text{usv}}(k_p+1) = \mathbf{A}_{\text{usv},d}\hat{\boldsymbol{x}}_{\text{usv}}(k_p), \tag{30}$$

$$\hat{\mathbf{P}}_{\text{usv}}(k_p+1) = \mathbf{A}_{\text{usv},d}\hat{\mathbf{P}}_{\text{usv}}(k_p)\mathbf{A}_{\text{usv},d}^{\mathsf{T}} + \mathbf{Q}_{\text{usv}}, \tag{31}$$

where $k_p = 0, 1, \ldots, N_p - 1$, $\hat{\boldsymbol{x}}_{\text{usv}}(0) = \boldsymbol{x}_{\text{usv}}(k)$, and $\hat{\mathbf{P}}_{\text{usv}}(0) = \mathbf{P}_{\text{usv}}(k)$.

## 4.2 Onboard USV Sensors

In practical scenarios, the UAV often operates at distance where its onboard sensors cannot provide sufficient data for USV state estimation. To address this issue, we assume a communication link between the UAV and USV, operating at least on 10 Hz. The USV sends sensor data to the UAV to roughly estimate the USV state. Subsequently, the UAV can fly to the proximity of the USV to use onboard UAV sensors, thereby increasing estimation and prediction precision. The first onboard USV sensor is a GPS device providing global position information. The second onboard USV sensor is an IMU that measures heading, angular velocity, and linear acceleration. These USV sensors are integrated within our MRS boat unit, which is placed on the USV board, as depicted in Fig. 4.

## 4.3 Onboard UAV Sensors

Establishing a fast and reliable communication link in the real world is challenging (Tran and Ahn, 2019). To deal with drop-outs of communication links, the UAV carries two onboard sensors that do not rely on a communication link. These onboard UAV sensors increase redundancy and enable usage of the system in various real-world conditions. Moreover, the two onboard sensory modalities demonstrate the system's ability to fuse data from multiple UAV and USV sensors that can be chosen according to the desired application.

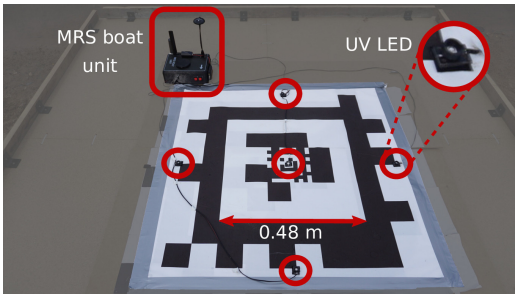


Figure 4: The USV board showing an AprilTag, UV LED (marked with red circles), and MRS boat unit, which contains GPS and IMU.

The first sensor is the AprilTag detector (Olson, 2011; Wang and Olson, 2016; Krogius et al., 2019). This vision-based system detects landmarks known as AprilTag in the camera image frame. The used landmark placed on USV board is shown in Fig. 4. In this custom landmark layout, a smaller AprilTag is placed within the empty space of the larger AprilTag, enabling detection from various distances (Krogius et al., 2019). The measured data from the AprilTag detector includes the position and orientation of the detected landmark. However, the AprilTag detector relies on sufficient lighting conditions to provide quality measurements due to its passive landmarks, which limits the system's usage, for example, in dark environments.

The second onboard UAV sensor is the UVDAR system (Walter et al., 2020; Walter et al., 2018b; Walter et al., 2018a), which detects blinking UltraViolet (UV) Light-Emitting Diodes (LEDs) placed on the target in camera image frames. The active blinking of the LEDs allows our solution to be used even in poor light conditions, such as darkness, where the AprilTag detector fails to provide sufficient measurements. The UV LEDs placed on the USV board are shown in Fig. 4. The UVDAR system provides measurements of the position and orientation of the target.

### 4.4 Trajectory Planner

The trajectory planner used for experimental verification is based on linear MPC, with detailed descriptions provided in (Prochazka, 2023). This planner utilizes estimated and predicted USV states (Sec. 4.1) to align the UAV trajectory with the motion of the USV. When the task is to follow the USV, the UAV maintains a desired distance above the USV board and promptly responds to changes in USV movement, such as those induced by waves. This responsiveness is important in applications where the UAV is tethered to the USV using a power supply cable to recharge UAV batteries (Talke et al., 2018). Failure of the UAV to react to the motion of the USV on waves poses a risk of the cable pulling the UAV and destabilizing it.

The landing task includes even more challenges. Firstly, the UAV must track the USV steadily. Subsequently, the UAV begins descending towards the USV board. In the final phase, the UAV lands on the USV board at a predefined vertical velocity relative to the USV velocity. This controlled descent is crucial for a safe landing, as it ensures that the vertical and touchdown velocity of the UAV are regulated throughout the entire maneuver, regardless of the vertical motion of the USV in the waves. Maintaining a static descending velocity despite the vertical motion of the USV carries a significant risk, as waves may push the USV towards the UAV, which significantly increases the UAV touchdown velocity, potentially causing damage to the UAV.

## 5 VERIFICATION

The proposed approach was first verified in simulations and subsequently deployed in real-world experiments. Moreover, we compare our results with those obtained using the state-of-the-art method (Polvara et al., 2018). The simulations were performed in a realistic robotic simulator Gazebo, extended by the Virtual RobotX (VRX) simulator (Bingham et al., 2019), which provides a realistic simulation of the harsh marine environment with large waves, as the UAV-USV collaboration in such conditions is our main motivation. A video attachment supporting the results of this paper is available at https://mrs.fel.cvut.cz/papers/towards-uav-usv-collaboration. The novelty of our approach lies in USV state estimation and prediction using our proposed novel USV model containing wave dynamics (Sec. 3). Therefore, we evaluate our estimation and prediction using Root Mean Square Error (RMSE). The Table 1 presents the RMSE of the estimated USV states using our approach computed from the performed simulations, in which the UAV follows and lands on the USV in harsh environment. The RMSE values are computed with respect to the sensors used for the estimation.

The estimation of position $(x, y, z)$ and corresponding linear velocities $(u, v, w)$ using GPS yields results with the largest RMSE. A better estimation for the states $(x, y, z)$ and $(u, v, w)$ compared to GPS is

Table 1: RMSE of the estimated USV states using the approach proposed in this paper with respect to the individual sensors.

| sensor | RMSE $(x,y,z)$ m | RMSE $(\phi,\theta,\psi)$ rad | RMSE $(u,v,w)$ m/s | RMSE $(p,q,r)$ rad/s |
|---|---|---|---|---|
| GPS | 0.989 | - | 0.985 | - |
| IMU | - | 0.011 | - | 0.536 |
| UVDAR | 0.425 | 0.124 | 0.977 | 1.034 |
| AprilTag | 0.088 | 0.052 | 0.848 | 0.606 |

Table 2: RMSE of the estimated USV states using the approach proposed in this paper compared to a state-of-the-art method.

| method | RMSE $(x,y,z)$ m | RMSE $(\phi,\theta,\psi)$ rad | RMSE $(u,v,w)$ m/s | RMSE $(p,q,r)$ rad/s |
|---|---|---|---|---|
| SOTA | 0.313 | 0.056 | 0.580 | 0.329 |
| our approach | 0.116 | 0.017 | 0.303 | 0.235 |

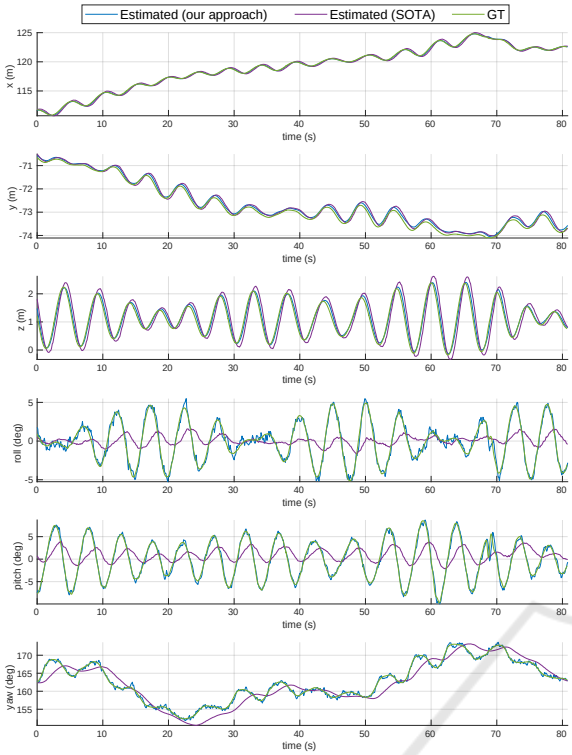


Figure 5: Estimated USV position $\boldsymbol{p} = (x, y, z)$ and orientation $\boldsymbol{\Theta} = (\phi, \theta, \psi)$ using the method proposed in this paper.

achieved through the UVDAR system. The RMSE for states $(x, y, z)$ is half the size when using the UVDAR system compared to the GPS, and for states $(u, v, w)$, the RMSE using the UVDAR system is slightly smaller than when using the GPS sensor. However, for the states $(\phi, \theta, \psi)$ and corresponding angular velocities $(p, q, r)$, the UVDAR yields the largest RMSE among all sensors. The most accurate estimation of the states $(\phi, \theta, \psi)$ is attained using IMU data, as indicated by its minimal RMSE. The smallest RMSE for $(x, y, z)$ and $(u, v, w)$ is achieved using the AprilTag detector. Moreover, the estimation of states $(\phi, \theta, \psi)$ and $(p, q, r)$ using the AprilTag detector results in a RMSE that is half as large as that of the UVDAR system. However, the RMSE of the AprilTag detector for states $(\phi, \theta, \psi)$ remains four and a half times larger than that of the IMU for the same states.

The Fig. 5 shows the estimated USV states from one of the many performed simulations, in which our approach fused data from all sensors. The graphs illustrate that all estimated states correspond to the Ground Truth (GT) values. The RMSE of estimated states using our approach is provided in the Table 2. We compared our approach with the most relevant state-of-the-art method (Polvara et al., 2018), which we call SOTA in this paper, as depicted in Fig. 5. Our

Table 3: RMSE of predicted and estimated USV states using the method proposed in this paper.

| USV states (our approach) | RMSE $(x, y, z)$ m | RMSE $(\phi, \theta, \psi)$ rad |
|---|---|---|
| predicted states | 0.737 | 0.196 |
| estimated states | 0.116 | 0.017 |

approach has smaller RMSE for all USV states (Table 2). The main difference is observed in the estimation of orientation $(\phi, \theta, \psi)$, where our approach achieves more than three times smaller RMSE compared to the SOTA. This substantial improvement in orientation estimation can be attributed to the overall UAV-USV collaboration system by the incorporation waves in the mathematical model and the fusion of data from multiple sensors, features lacking in SOTA. The impact of this difference is evident in Fig. 5 in the estimation of heave $z$, roll $\phi$, and pitch $\theta$, where our approach exhibits closer alignment with GT values compared to SOTA.

The predicted USV states $(x, y, z, \phi, \theta, \psi)$ from one of the performed simulations are shown in Fig. 6. The two-second predictions are computed every two seconds. The figure illustrates that the predictions initially deviate more from the GT values at the beginning of the simulation. However, as the estimation progresses over time, the predicted USV states become increasingly accurate. The RMSE of predictions for states $(x, y, z)$ proposed in Table 3 corresponds to the RMSE of estimation of these states using only the GPS sensor (Table 1). The RMSE of predictions for states $(\phi, \theta, \psi)$ corresponds to the RMSE of these states estimated using UVDAR system (Table 1). These results demonstrate the applicability of computed predictions to UAV trajectory planner.

## 5.1 Real-World Experiments

To analyze the real-world performance and to show robustness to real uncertainties and disturbances, we deployed the presented approach in real-world experiments. During the first set of real-world experiments, the overall system demonstrated robust performance, allowing the UAV to repeatedly follow the USV and land on the USV's deck. In these experiments, the USV was manually forced to perform wave motions, as depicted in Fig. 7 (a). The UAV was equipped with an onboard computer, GPS sensor, and cameras for the AprilTag detector and the UVDAR system (see (Hert et al., 2023; Hert et al., 2022) for details). The USV's deck, featuring the AprilTag and UV LEDs, is detailed in Fig. 4. Additionally, the USV carried the MRS boat unit containing IMU and GPS sensors. The detailed description of the used UAV and USV

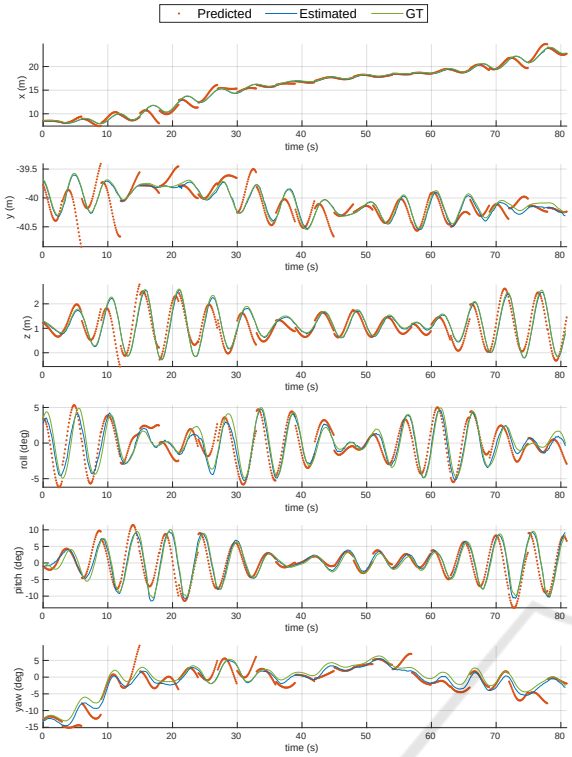


Figure 6: Predicted USV position $\boldsymbol{p} = (x, y, z)$ and orientation $\boldsymbol{\Theta} = (\phi, \theta, \psi)$ using the method proposed in this paper.

sensors is provided in Sec. 4.2 and 4.3.

The estimated USV states from one of the performed real-world experiments are depicted in Fig. 8. Initially, the UAV approached the USV while USV states were estimated using received GPS and IMU data. Subsequently, the UAV onboard sensors improved the estimation, as evident in the graphs of USV position $(x, y, z)$ (Fig. 8). Then, the UAV followed the USV, which performed artificially induced wave motion that can be noticed especially in roll and pitch graphs. The pitch was affected by waves from 37 s to 130 s and from 200 s to 264 s, while the roll was affected from 130 s to 200 s.

The UAV was also able to successfully land on the USV, as depicted in Fig. 7 (b). The USV was towed by another boat, while the UAV followed it using a trajectory planner (Sec. 4.4) that utilized estimated and predicted USV states. When the conditions for


Figure 7: The figure depicts snapshots from the performed real-world experiments, in which the UAV (marked with a red circle) followed the USV (a) and landed on the USV (b).

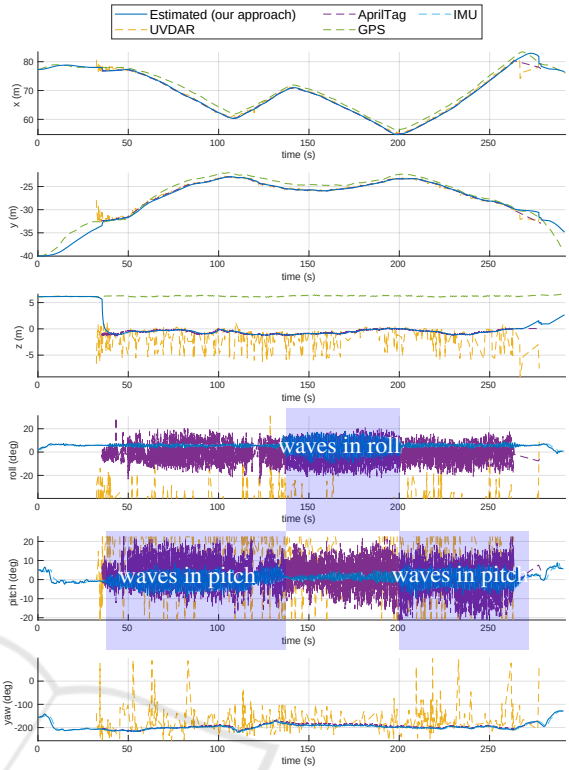


Figure 8: Estimated USV states using our approach in one of the performed real-world experiments.

a safe landing were met, the UAV initiated a landing maneuver, which was successfully completed within 6 s.

## 6 CONCLUSION

In this paper, we introduce a novel onboard UAV approach designed to facilitate tight collaboration between UAV and USV in harsh marine environments, such as following or landing maneuvers. The main contribution of the proposed solution is the USV state estimator and predictor, operating in 6 DOFs, which uses our novel mathematical USV model incorporating wave dynamics. The state estimator fuses data from multiple UAV and USV sensors, ensuring accurate estimation across various real-world conditions. Subsequently, the estimated USV states are fed into the state predictor, which utilizes the mathematical USV model to predict future USV states in 6 DOFs. We verified the overall system through extensive simulations and compared the results of the proposed approach with the state-of-the-art method. The proposed approach was also deployed in real-world experiments, where the UAV was able to repeatedly follow the USV and land on the USV's deck. Future

work will focus on developing a nonlinear mathematical model of the USV to better capture its dynamics on a wavy water surface. Moreover, the proposed approach is planned to be integrated into an autonomous UAV-USV team designed for garbage removal and water quality monitoring.

## ACKNOWLEDGEMENTS

This work was funded by the Czech Science Foundation (GAČR) under research project no. 23-07517S, by the European Union under the project Robotics and advanced industrial production (reg. no. CZ.02.01.01/00/22_008/0004590), and by CTU grant no SGS23/177/OHK3/3T/13.

## REFERENCES

Abujoub, S., McPhee, J., Westin, C., and Irani, R. A. (2018). Unmanned aerial vehicle landing on maritime vessels using signal prediction of the ship motion. In *OCEANS 2018 MTS/IEEE Charleston*, pages 1–9.

Aissi, M., Moumen, Y., Berrich, J., Bouchentouf, T., Bourhaleb, M., and Rahmoun, M. (2020). Autonomous solar usv with an automated launch and recovery system for uav: State of the art and design. In *2020 IEEE 2nd International Conference on Electronics, Control, Optimization and Computer Science (ICECOCS)*, pages 1–6.

Aniceto, A. S., Biuw, M., Lindstrøm, U., Solbø, S. A., Broms, F., and Carroll, J. (2018). Monitoring marine mammals using unmanned aerial vehicles: quantifying detection certainty. *Ecosphere*, 9(3):e02122.

Baca, T., Petrlik, M., Vrba, M., Spurny, V., Penicka, R., Hert, D., and Saska, M. (2021). The MRS UAV System: Pushing the Frontiers of Reproducible Research, Real-world Deployment, and Education with Autonomous Unmanned Aerial Vehicles. *Journal of Intelligent & Robotic Systems*, 102(26):1–28.

Bingham, B., Aguero, C., McCarrin, M., Klamo, J., Malia, J., Allen, K., Lum, T., Rawson, M., and Waqar, R. (2019). Toward maritime robotic simulation in Gazebo. In *Proceedings of MTS/IEEE OCEANS Conference*, Seattle, WA.

Fossen, T. I. (2011). *Handbook of Marine Craft Hydrodynamics and Motion Control*. John Wiley & Sons, United Kingdom, first edition edition.

Gupta, P. M., Pairet, E., Nascimento, T., and Saska, M. (2023). Landing a uav in harsh winds and turbulent open waters. *IEEE Robotics and Automation Letters*, 8(2):744–751.

Han, Y. and Ma, W. (2021). Automatic monitoring of water pollution based on the combination of uav and usv. In *2021 IEEE 4th International Conference on Electronic Information and Communication Technology (ICEICT)*, pages 420–424.

Hert, D., Baca, T., Petracek, P., Kratky, V., Penicka, R., Spurny, V., Petrlik, M., Vrba, M., Zaitlik, D., Stoudek, P., Walter, V., Stepan, P., Horyna, J., Pritzl, V., Sramek, M., Ahmad, A., Silano, G., Bonilla Licea, D., Stibinger, P., Nascimento, T., and Saska, M. (2023). MRS Drone: A Modular Platform for Real-World Deployment of Aerial Multi-Robot Systems. *Journal of Intelligent & Robotic Systems*.

Hert, D., Baca, T., Petracek, P., Kratky, V., Spurny, V., Petrlik, M., Vrba, M., Zaitlik, D., Stoudek, P., Walter, V., Stepan, P., Horyna, J., Pritzl, V., Silano, G., Bonilla Licea, D., Stibinger, P., Penicka, R., Nascimento, T., and Saska, M. (2022). MRS Modular UAV Hardware Platforms for Supporting Research in Real-World Outdoor and Indoor Environments. In *2022 International Conference on Unmanned Aircraft Systems (ICUAS)*, pages 1264–1273. IEEE.

Kalman, R. E. (1960). A new approach to linear filtering and prediction problems. *Journal of Basic Engineering*, 82(1):35–45.

Keller, A. and Ben-Moshe, B. (2022). A robust and accurate landing methodology for drones on moving targets. *Drones*, 6(4).

Krogius, M., Haggenmiller, A., and Olson, E. (2019). Flexible layouts for fiducial tags. In *IEEE/RSJ International Conference on Intelligent Robots and Systems (IROS)*.

Lee, S., Lee, J., Lee, S., Choi, H., Kim, Y., Kim, S., and Suk, J. (2019). Sliding mode guidance and control for uav carrier landing. *IEEE Transactions on Aerospace and Electronic Systems*, 55(2):951–966.

Marconi, L., Isidori, A., and Serrani, A. (2002). Autonomous vertical landing on an oscillating platform: an internal-model based approach. *Automatica*, 38(1):21–32.

Meng, Y., Wang, W., Han, H., and Ban, J. (2019). A visual/inertial integrated landing guidance method for uav landing on the ship. *Aerospace Science and Technology*, 85:474–480.

Murphy, R., Stover, S., Pratt, K., and Griffin, C. (2006). Cooperative damage inspection with unmanned surface vehicle and micro unmanned aerial vehicle at Hurricane Wilma. In *2006 IEEE/RSJ International Conference on Intelligent Robots and Systems*, pages 9–9.

Murphy, R. R., Steimle, E., Griffin, C., Cullins, C., Hall, M., and Pratt, K. (2008). Cooperative use of unmanned sea surface and micro aerial vehicles at Hurricane Wilma. *Journal of Field Robotics*, 25(3):164–180.

Olson, E. (2011). AprilTag: A robust and flexible visual fiducial system. In *IEEE International Conference on Robotics and Automation (ICRA)*, pages 3400–3407. IEEE.

Polvara, R., Sharma, S., Wan, J., Manning, A., and Sutton, R. (2018). Vision-based autonomous landing of a quadrotor on the perturbed deck of an unmanned surface vehicle. *Drones*, 2(2).

Prochazka, O. (2023). Trajectory planning for autonomous landing of a multirotor helicopter on a boat. Master's thesis, Faculty of Electrical Engineering, Czech Technical University in Prague.

Román, A., Tovar-Sánchez, A., Gauci, A., Deidun, A., Caballero, I., Colica, E., D'Amico, S., and Navarro, G. (2023). Water-quality monitoring with a uav-mounted multispectral camera in coastal waters. *Remote Sensing*, 15(1).

Talke, K. A., De Oliveira, M., and Bewley, T. (2018). Catenary tether shape analysis for a uav - usv team. In *2018 IEEE/RSJ International Conference on Intelligent Robots and Systems (IROS)*, pages 7803–7809.

Tran, Q. V. and Ahn, H.-S. (2019). Multi-agent localization of a common reference coordinate frame: An extrinsic approach. *IFAC-PapersOnLine*, 52(20):67–72. 8th IFAC Workshop on Distributed Estimation and Control in Networked Systems NECSYS 2019.

Venugopalan, T. K., Taher, T., and Barbastathis, G. (2012). Autonomous landing of an unmanned aerial vehicle on an autonomous marine vehicle. In *2012 Oceans*, pages 1–9.

Walter, V., N.Staub, Saska, M., and Franchi, A. (2018a). Mutual localization of UAVs based on blinking ultraviolet markers and 3D time-position Hough transform. In *14th IEEE International Conference on Automation Science and Engineering (CASE 2018)*.

Walter, V., Saska, M., and Franchi, A. (2018b). Fast mutual relative localization of UAVs using ultraviolet LED markers. In *2018 International Conference on Unmanned Aircraft System (ICUAS 2018)*.

Walter, V., Vrba, M., and Saska, M. (2020). On training datasets for machine learning-based visual relative localization of micro-scale UAVs. In *2020 IEEE International Conference on Robotics and Automation (ICRA)*, pages 10674–10680.

Wang, J. and Olson, E. (2016). AprilTag 2: Efficient and robust fiducial detection. In *IEEE/RSJ International Conference on Intelligent Robots and Systems (IROS)*.

Xu, Z.-C., Hu, B.-B., Liu, B., Wang, X., and Zhang, H.-T. (2020). Vision-based autonomous landing of unmanned aerial vehicle on a motional unmanned surface vessel. In *2020 39th Chinese Control Conference (CCC)*, pages 6845–6850.

Yang, L., Liu, Z., Wang, X., Wang, G., Hu, X., and Xi, Y. (2021). Autonomous landing of a rotor unmanned aerial vehicle on a boat using image-based visual servoing. In *2021 IEEE International Conference on Robotics and Biomimetics (ROBIO)*, pages 1848–1854.

Zhang, H.-T., Hu, B.-B., Xu, Z., Cai, Z., Liu, B., Wang, X., Geng, T., Zhong, S., and Zhao, J. (2021). Visual navigation and landing control of an unmanned aerial vehicle on a moving autonomous surface vehicle via adaptive learning. *IEEE Transactions on Neural Networks and Learning Systems*, 32(12):5345–5355.